

# Tunneling induced electron transfer between separated protons

Patricia Vindel-Zandbergen and Christoph Meier  
*Laboratoire Collisions, Agrégats et Réactivité, UMR 5589,  
 IRSAMC, Université Paul Sabatier, 31062 Toulouse, France*

Ignacio R. Sola  
*Departamento de Química Física, Universidad Complutense, 28040 Madrid, Spain\**

We study electron transfer between two separated nuclei using local control theory. By conditioning the algorithm in a symmetric system formed by two protons, one can favored slow transfer processes, where tunneling is the main mechanism, achieving transfer efficiencies close to unity assuming fixed nuclei. The solution can be parametrized using sequences of pump and dump pi pulses, where the pump pulse is used to excite the electron to a highly excited state where the time for tunneling to the target nuclei is on the order of femtoseconds. The time delay must be chosen to allow for full population transfer via tunneling, and the dump pulse is chosen to remove energy from the state to avoid tunneling back to the original proton. Finally, we study the effect of the nuclear kinetic energy on the transfer efficiency. Even in the absence of relative motion between the protons, the spreading of the nuclear wave function is enough to reduce the yield of electronic transfer to less than one half.

## I. INTRODUCTION

Quantum control can be described as a dynamic process that prepares coherent superpositions of Hamiltonian eigenstates manipulating the amplitudes and relative phases [1–3]. When this wave function involves several electronic states, the phases typically oscillate in the sub-femtosecond (hence attosecond) time scale. However, this is not always the case, as energy differences between Rydberg states vary on the order of  $\sim 1/n$  Hartrees, which can be relatively small for large  $n$ . Hence the period of motion associated to these phase oscillations can be of the order of femtoseconds or larger [4, 5].

In molecules, other scenarios of electronic changes associated to the femtosecond scale exists whenever the electronic states become quasi-degenerate. This is the case in the proximity of conical intersections, [6–8] and it is also the case in the dissociation limit, where many molecular electronic states correlate with the same atomic (or fragment) electronic states. The latter situation is particularly interesting in symmetric arrangements. Then the initial and target wave function may only differ by the phase of the initial superposition, which identifies different isomers that can be converted via tunneling [9, 10]. However, the similar time scales of vibrational and electronic motion can make the control of the electronic processes particularly sensitive to the nuclear displacements or even require fully correlated electron-nuclear motion [11, 12]. Electronic processes in the attosecond regime may be more protected against vibrational motion, particularly if the process occurs a single time [13]. However, the effect of vibrational decoherence must still be carefully studied [14, 15].

In this work we investigate electronic transfer between

two separated protons, where the electron is initially in a single proton, breaking the symmetry of the system. We have recently shown that a local control (LC) approach [16–18] can be used to find ultrashort pulses that induce electron transfer in very few femtoseconds, yielding pulses characterized by a prominent (very intense) spike that maximizes the probability of retrapping the electron at the desired proton, after moving and spreading in the ionizing continuum [13]. In principle there are infinite solutions of the control problem, and the LC method is flexible enough to find different types of solutions. In this work we show that for particular choices of observables, varying the initial conditions can lead to optimal control of electron transfer that explore a different control mechanism, characterized by slow electron transfer via tunneling.

The paper is organized as follows. In section II we introduce the model Hamiltonian and describe the numerical methods used to simulate and control the dynamics. In section III we find the control mechanism that implies slow electron transfer between two protons largely separated via tunneling. In section IV we study the role of the nuclear motion in the control of the electron transfer in this timescale. Finally, section V is the conclusions.

## II. NUMERICAL METHODS

We need to use a consistent model for treating both continuum and bound electronic states in a system with a single electron and two protons. As a first approximation, we use a  $1 + 1D$  Hamiltonian, including the internuclear distance  $R$  and the electron separation to the center of mass  $z$ , where the electron is constrained to move in the molecular axis. For this reduced dimensional study the inter-particle interaction is modeled by a soft-core Coulomb potential [19]. In the presence of a linearly polarized external field,  $\mathcal{E}(t)$ , and neglecting

---

\*Electronic address: isola@quim.ucm.es

small mass polarization terms, the Hamiltonian in the length gauge is (atomic units are used throughout unless otherwise stated)

$$H = -\frac{1}{2} \frac{\partial^2}{\partial z^2} - \frac{1}{M} \frac{\partial^2}{\partial R^2} + V(z, R) + z\mathcal{E}(t) \quad (1)$$

where  $M$  is the mass of the proton, with the soft-core Coulomb potential

$$V(z, R) = -\frac{1}{\sqrt{1 + (z - R/2)^2}} - \frac{1}{\sqrt{1 + (z + R/2)^2}} + \frac{1}{R} \quad (2)$$

This model has been extensively applied as a first qualitative step to analyze ionization processes in  $\text{H}_2^+$  and high-harmonic spectra [20, 21], as well as electron-nuclear dynamics [11, 12, 22, 23].

Initially, we assume a fixed nuclei approximation, where an hydrogen atom and a proton are largely separated. In Section III we select results for fixed internuclear distances of 10 and 20 a.u. We achieve electron transfer applying LCT. The objective is mathematically expressed as the population in a target state  $|\psi_f\rangle$ , constructed as a wave function localized at the proton where we want the electron to be recaptured [24, 25]. Therefore, the control field depends on the projection on a target state

$$\mathcal{E}(t) = \lambda \Im [\langle \Psi(t) | \mu | \psi_f \rangle \langle \psi_f | \Psi(t) \rangle] \quad (3)$$

where  $\Im$  stands for the imaginary part and  $\Psi(t)$  is the wave function of the system. Here  $\lambda$  enters as a free parameter to be found numerically, that characterizes the strength of the laser interaction.

In finding the local control field with Eq.(3), the projection operator  $P_t = |\psi_{R_1}\rangle\langle\psi_{R_1}|$  must commute with the Hamiltonian of the system [17]. Therefore, the target wave function must be an eigenfunction of the Hamiltonian. However, if the separation of the protons is not large enough, the localized wave functions are not true eigenstates, as the tunneling time cannot be neglected. One way of solving this problem is to add a very small static field component,  $\mathcal{E}_{DC}$ , that breaks the symmetry of the Hamiltonian, such that the effective potential is tilted,  $V_{\text{tilted}}(z) = V(z) + z\mathcal{E}_{DC}$ . Then the target and the initial states are the ground or first excited electronic wave functions of the Hamiltonian with the DC component localized at the desired proton. The initial state,  $\psi_L$ , is localized at the left potential well and  $\psi_R$  is the target state, localized at the right potential well.

By making  $\mathcal{E}_{DC}$  small enough, the tilted potential has no significant impact on the search of the local control field for large internuclear distances ( $R \geq 20$  a.u.). However, the DC component is an essential ingredient in the control of electron localization at smaller proton separations.

In our simulations, the initial state is created by exciting the  $\text{H}_2^+$  molecule, that is,  $\psi_L$  is multiplied by an

exponential factor that gives an initial momentum in the positive direction

$$\Psi(z, 0) = \psi_{L_1}(z) e^{ik_e z} \quad (4)$$

In addition, to initiate the LCT approach one needs a small "seed" of population in the right potential well (the target state), which we fix as  $\approx 0.3\%$ . Once the local control field is found this "seeded" population is no longer needed, and the simulations shown in the results imply 100% population in the ground (localized) state at initial time.

Numerical results are obtained by solving the TDSE with the Split-Operator method [26–28] with time steps ranging from  $\Delta t = 0.1$  to 0.01 a.u. depending on the simulation. A grid of 1024 points spanning from  $z = -80$  to  $z = 80$  a.u. is used for the electronic coordinate. Imaginary ("optical") potentials [29, 30] absorb the outgoing wave functions avoiding reflection on the grid boundaries and allowing to measure the ionization probability. The eigenstates  $\psi_{L,R}$  are computed using the Fourier Grid Hamiltonian method [31]. The dynamical mechanism of the transfer is studied by analyzing the approximate phase-space representation of the wave functions at different times, using the Husimi transformation [32].

Finally, to study the role of the nuclear motion in the control of the electron transfer, 1 + 1D calculations were performed using the full Hamiltonian of Eq.(1). The initial wave packet is the product of the electronic wave function times a nuclear Gaussian wave packet  $\psi_{\text{nuc}}(R)$ , centered at the left nuclei. In these simulations we use a grid of 1024 points ranging from  $R = 0.1$  to  $R = 150$  a.u. for the nuclear coordinate and 256 points, from  $z = -80$  to  $z = 80$  a.u., for the electronic coordinate.

### III. SLOW ELECTRON TRANSFER

#### The tunneling mechanism

We first study electron transfer when the electron starts with a small positive average momentum. The initial wave function, localized at the left potential, has an initial momentum of  $k_e = 0.001$  a.u. [see Eq.(4)]. Under these conditions, best results are obtained for nuclei separated less than 20 a.u. The results of a typical LCT calculation are shown in Fig.1(a) and (b) for fixed nuclei separated  $R = 10$  and  $R = 20$  a.u. In the latter case, a free electron transfer (without any acting force) would take roughly  $t = R/k_e = 2 \cdot 10^4$  a.u.  $\approx 500$  fs. The initial kinetic energy is not enough to overcome the net attractive force of the potential (that is, to overcome the Coulomb barrier between the protons), so that in principle the pulse must act to excite the electron and then to retrap it.

We have used an LCT approach based on the projection operator on a target wave function that is the lowest energy eigenfunction localized on the right well of the

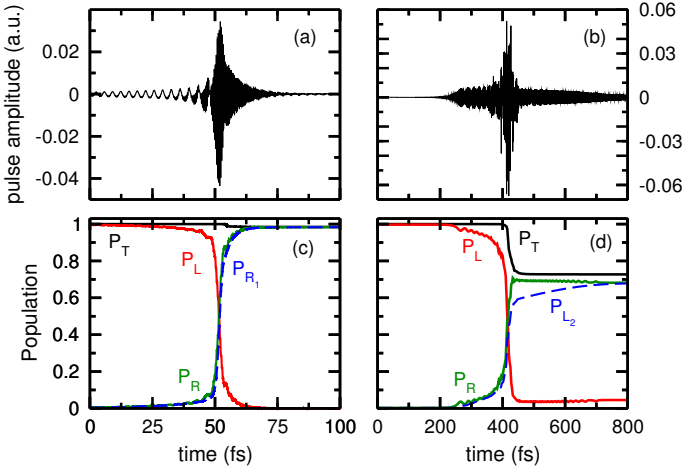


FIG. 1: Laser control fields and population dynamics for an internuclear distance of 10 a.u. [(a) and (c)] and 20 a.u. [(b) and (d)], when tunneling is the main mechanism responsible for electron transfer.

tilted potential. The calculations were performed using a static field of  $\mathcal{E}_{DC} = -5 \cdot 10^{-3}$  a.u. and  $\mathcal{E}_{DC} = -2 \cdot 10^{-5}$  a.u., for  $R = 10$  and  $R = 20$  a.u., respectively. Best results were obtained with  $\lambda = 0.2$  for  $R = 10$  a.u. and  $\lambda = 2.8$  for  $R = 20$  a.u. in Eq.(3).

Fig.1(a) and (b) show the optimal fields for  $R = 10$  a.u. and  $R = 20$  a.u., while the (c) and (d) panels represent the respective population dynamics partitioned into left and right domains

$$P_D(t) = |\langle \Psi(z, t) | \Psi(z, t) \rangle_{z \in D}|^2 \quad (5)$$

where  $D$  is  $(-L/2, 0)$  or  $(0, L/2)$  (with  $L$  the grid size) for the left and right domains, respectively. Also shown is the yield of the process, measured as the overlap of the wave function with the target state,

$$P_{R_1}(t) = |\langle \psi_{R_1} | \Psi(z, t) \rangle|^2 \quad (6)$$

As observed, for  $R = 10$  a.u., full electron transfer is achieved with  $\sim 0.08\%$  population remaining in the left potential well. The final population in the right potential well is completely localized in the target state,  $P_{R_1}/P_R = 1$ , and there is no population loss due to ionization. For  $R = 20$  a.u., again the electron transfer is almost perfect, with  $\sim 6\%$  population in the left hydrogen. The final population is localized in the target state, as  $P_{R_1}/P_R = 0.99$ , while the remaining population (less than 30%) is lost as ionization.

To interpret the mechanism under the electron transfer process, it is important to notice that the average energy of the electron never exceeds the energy of the Coulomb barrier between the two protons in the soft-core Coulomb potential. In addition, at these internuclear distances, the tunneling times between localized states are within

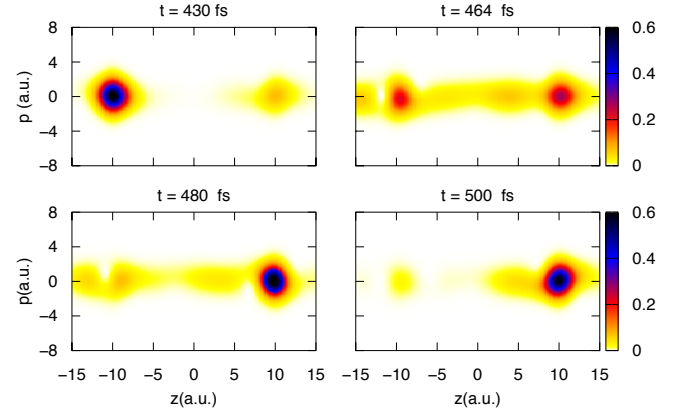


FIG. 2: Husimi distributions at different times of the electron transferred from the left to the right proton, for a fixed internuclear distance of  $R = 20$  a.u.

the time-scale of the control process. A rough calculation for  $R = 20$  a.u. gives  $t_1 \approx 3$  ps for population inversion between the ground localized states,  $\psi_{L_1}$  and  $\psi_{R_1}$ , and  $t_2 \approx 250$  fs for population inversion between the first excited localized states in each well,  $\psi_{L_2}$  and  $\psi_{R_2}$ . With  $R = 10$  a.u., the population inversion between  $\psi_{L_1}$  and  $\psi_{R_1}$  is  $t_1 \approx 100$  fs. For the soft-core model other excited states have energies above the Coulomb barrier. Roughly, we propose the following mechanism as the key process governing the electron transfer controlled by the LC pulse: First, as a net positive momentum is given to the electron initially, the electron finds itself distributed between the excited states of the left hydrogen with energies below the continuum. The electron is then transferred to the right proton by tunneling. Finally, the pulse takes energy away from the electron sitting in the right proton, effectively stopping the back-tunneling process to the left proton.

To help visualizing the process we calculate the Husimi distributions of the wave functions at different times. Fig.2 shows the Husimi plots of the electron wave function at the time the electron transfer is happening for  $R = 20$  a.u. As observed, the momentum distribution is localized around zero and does not change, implying that the electron is not reaching the continuum while it moves to the right potential well. These distributions correspond to a tunneling mechanism, where the electron density starts to “disappear” from the left hydrogen atom and “appears” at the proton on the right.

Since tunneling is the main mechanism behind the control process, in the following we impose such mechanism by choosing sine squared ( $\sin^2(\pi(t-t_0)/\tau)$ ) shaped pulses that lead the different steps proposed above for the electron transfer. The peak amplitude and pulse durations ( $\tau$ ) are estimated numerically by trial and error to maximize the overall yield. The idea is to use two laser pulses tuned to the first electronic transition, time-delayed by

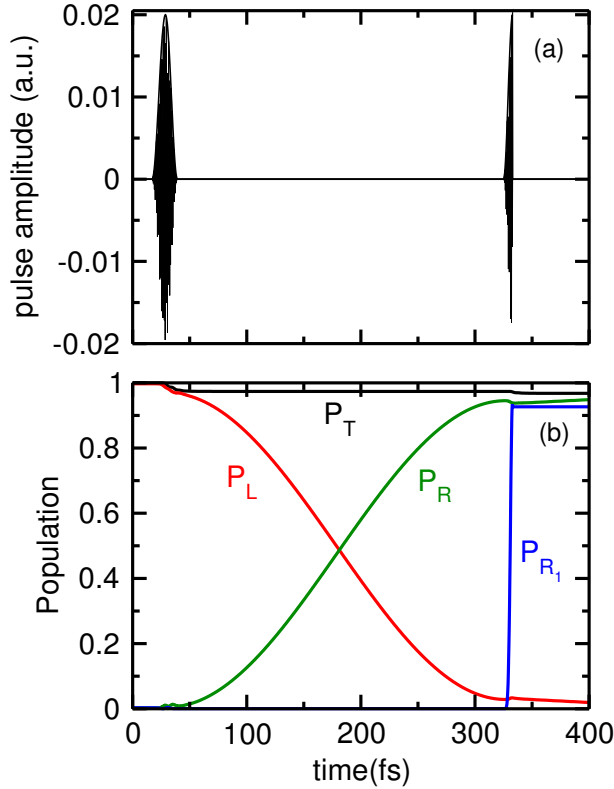


FIG. 3: Population dynamics and laser pulses used in the "four-state" control scheme.  $P_{L/R}$  refers to the probability of finding the electron at the left/right of the center of mass of the system,  $P_T$  is the norm of the wave function (deviations from unity are due to ionization) and  $P_{R_1}$  is the population in the target state.

$t_2$ , the time it takes for tunneling in the first excited localized states. This is a "four-state" scheme where only the localized ground states ( $\psi_{L_1}$  and  $\psi_{R_1}$ ) and first excited states ( $\psi_{L_2}$  and  $\psi_{R_2}$ ) participate in the dynamics. In this control scenario we have used  $k_e = 0$ . Fig.3(a) and (b) show the laser pulses and the population dynamics. The first laser pulse that produces population inversion from  $\psi_{L_1}$  to  $\psi_{L_2}$  is equivalent to a  $\pi$  pulse of  $\sim 20$  fs duration, 0.02 a.u. pulse amplitude and  $\omega = 0.39$  a.u. The second laser pulse that de-excites the electron from  $\psi_{R_2}$  to  $\psi_{R_1}$  is also a  $\pi$  pulse of  $\sim 10$  fs duration, 0.02 a.u. pulse amplitude and  $\omega = 0.39$  a.u. The yield of population inversion for the second pulse is only slightly lower than 1. Using this scheme, one can completely avoid ionization ( $\approx 2\%$ ). In fig.4 we observe the propagation of the electronic wave packet, that shows the mechanism of the "four-states" scheme.

For  $R = 10$  a.u. the mechanism is even simpler. Since the tunneling time in the ground state is  $t_1 = 100$  fs, starting from the localized state at the left hydrogen, we just need to wait enough time for the electron to completely transfer to the right proton, without the action of an external laser field. However, in this case, the op-

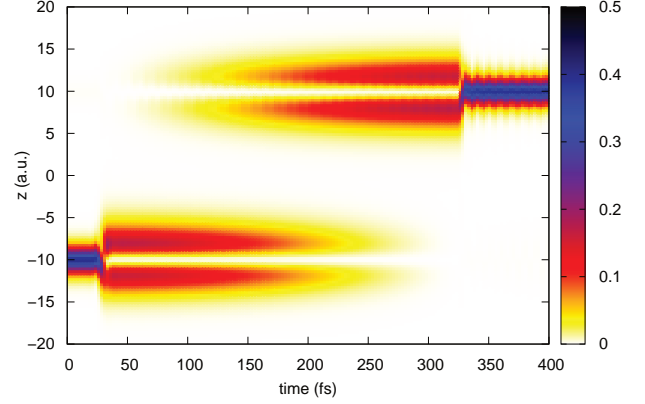


FIG. 4: Dynamics of the electron density using the "four-state" control scheme.

posite process also occurs, so that the electron cannot remain localized.

In summary, electron transfer between protons that are separated by moderately large distances is possible by means of a slow transfer process, where tunneling below the internal barrier is the predominant mechanism. Tunneling can be made the sole mechanism responsible for the process. In this case, however, local control theory is not required, as analytic pulses, or even no external field, can lead to the same final results. The tunneling mechanism can not be used effectively when the internuclear distance increases, as the tunneling time increases exponentially and one needs to selectively excite the electron to Rydberg states ever closer to the continuum, a process that is difficult by itself. In addition, as we show in the next section, the nuclear dynamics acts as a very strong perturbation source that affects the yield of the process.

### The role of the nuclear motion

The fixed nuclei approximation is valid as long as the electronic processes occur in a time-scale much faster than that of the nuclear motion. In the slow electron transfer mechanism, the transfer times are of the order or larger than typical vibrational periods. Here, we analyze how the nuclear motion affects the yield of the tunneling process. We use the optimal pulses found in the fixed-nuclei LCT approach, as well as the analytic pulses of the "four-state" scheme and apply them on a full 2-D (or (1 + 1D)) calculation considering different initial nuclear wave functions. The effect of the initial nuclear kinetic energy is considered in two different ways: by studying the effect of the width of the initial Gaussian nuclear wave function and by adding a net momentum in the positive or negative direction. However, we do not directly apply the LCT approach to the (1 + 1)D TDSE,



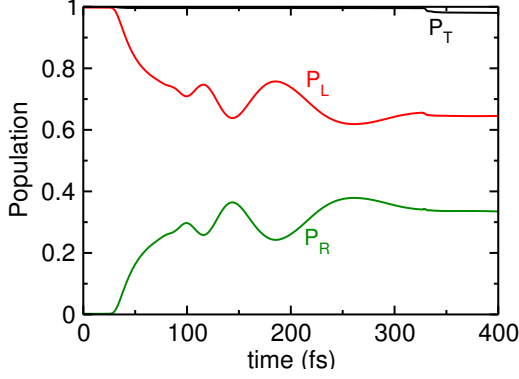


FIG. 5: Population dynamics in a 2-D calculation with zero average initial momentum using the "four-state" scenario.

that is, the pulses are not directly optimized taking into account the nuclear motion.

As a representative example, fig.5 shows the effect of the nuclear motion over the population dynamics for  $R = 20$  a.u., when the analytic pulses of the 1-D "four-states" scenario are used in a 2-D calculation and no net average momentum is given to the nuclei. Although some population transfer is achieved and ionization is also avoided, the effect of the nuclear motion completely influences the photoassociation process. Now, only  $\sim 30\%$  population remains at the right Hydrogen and the electron transfer mainly occurs in the first 150 fs, but the transfer mechanism is the same as in the 1-D situation. As observed in fig.7, the 2-D wave packet initially spreads along the internuclear coordinate during the first 20 fs. Then, the first laser pulse excites the electron to  $\psi_{L_2}$  in the left hydrogen (negative  $z$  values). Because at  $R = 20$  a.u. there is a small attractive force between the nuclei, even when no net momentum is given, the nuclei approach. Now, the tunneling time is lower since the wave function is moving to lower internuclear distances (breaking the degeneracy of the electronic wave functions due to the internal barrier), and the population transfer mainly finishes at  $t \sim 60$  fs. Between 325 and 330 fs the population inversion occurs from the excited to the ground state of the right proton, when the second laser pulse is acting. Finally, we obtain an electron population distributed in the two potential wells that spreads along the internuclear distance, but mainly around  $R = 20$  a.u.

Fig.6 shows the effect of the nuclear motion as the ratio between the 2-D and the 1-D results for the yield of the process  $P_R(\infty)$  (the probability of being localized at the right proton at final time) as well as for the remaining (not ionized) population  $P_T(\infty)$ . In Fig.6(a) we fix the initial width of the nuclear Gaussian wave packet at  $\sigma = 0.31$  a.u. and we consider the effect of positive or negative nuclear momentum. In fig.6(b) the net momentum is zero and only the width of the initial Gaussian

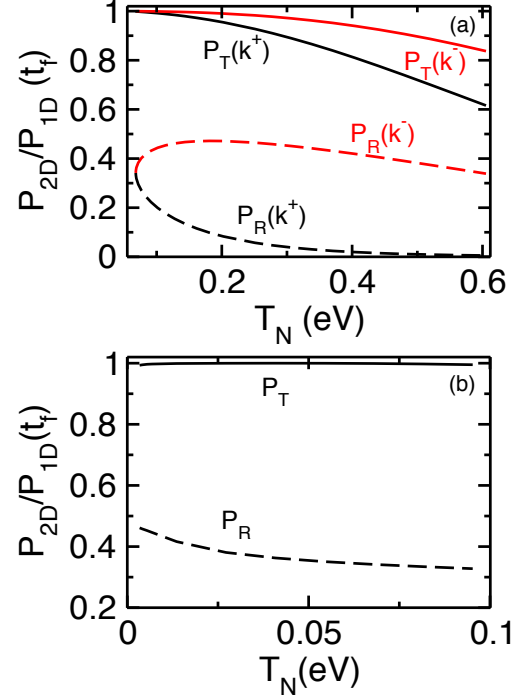


FIG. 6: Variation of the probability of finding the electron at the right proton at final time  $P_R$  and the norm of the wave function  $P_T$  as a function of the initial nuclear kinetic energy (a) depending on the initial average momentum given to the nuclei (positive,  $k_n^+$ , or negative,  $k_n^-$ ) and (b) depending on the initial width of the nuclear wave function, assuming zero average initial momentum

wave packet is changed. As a first insight, one can observe the yield of population transfer decreases to  $\sim 30\%$  when no initial momentum is given to the nuclei, but the total population remains as in the 1-D calculations.

Also, we can notice differences in the variation of the final population depending on the sign of the initial nuclear momentum. The total population decreases as the initial kinetic energy increases for both positive and negative momenta, but the degree of population loss is bigger in the positive case. As well, we can appreciate this behavior in the population transfer to the right potential well for positive values of the nuclear momentum. However, when considering the negative case, initially there is an increase in the electron transfer to the right proton for small initial kinetic energies of the nuclei. Then, the yield decreases but not as drastically as for positive values.

These results can be explained by considering the potential energy curves of the second and third excited states where the tunneling is happening [fig.8 (a)] and the variation of the average of the internuclear distance with the initial nuclear kinetic energy [fig.8 (b)]. When we apply a negative momentum, the nuclei start to get closer, so the tunneling time decreases, therefore, initially

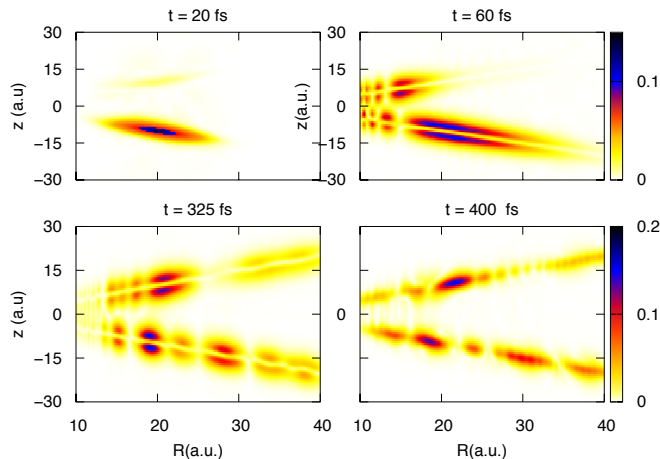


FIG. 7: Snapshots of the electron density at different times. The electron transfer corresponds to the "four-state" scheme described in the 1D approach, where an initial laser pulse of  $\sim 20$  fs duration, 0.02 a.u. amplitude and  $\omega = 0.39$  a.u., is used to excite the electron to the first excited state localized in the left hydrogen. A second laser pulse with same amplitude and frequency but  $\sim 10$  fs duration de-excites the electron to the ground state localized in the right nucleus. The time-delay between these two  $\pi$  pulses corresponds to the tunneling time between the two first localized excited states. Although the wave packet spreading along the internuclear distance is a main issue affecting the photoassociation process, some degree of population transfer is achieved and ionization is avoided.

the electron transfer increases. But, from kinetic values larger than  $\sim 0.15$  eV the electron transfer remains constant, regardless of the increase of the initial nuclear momentum. The decrease of the population in the right potential is due to the total population loss by ionization.

When considering positive values of the initial momentum, as the nuclei separate, the energy difference between the excited states decreases and the tunneling time increases, lowering the population transfer, finally even avoiding photoassociation.

Regarding the nuclear potential energy curves around  $R = 20$  a.u. [fig.8(a)], for lower values of the internuclear distance, the energy difference between states increases, so the overlap between the second and third excited states must decrease. On the other hand, as we move to larger values of  $R$ , the energy difference becomes nearly zero, so the excited states are now degenerated states and the overlap between them is close to 1.

Resuming, for negative values of the initial nuclear momentum, the population transfer increases as the nuclei approximate. The internuclear distance decreases so the energy difference between the excited states increases and the tunneling time diminishes. Positive values of initial kinetic energies, imply a rise of the internuclear distance as the nuclei are separating, so the energy difference between the excited states is reduced. The tunneling time increases so the population transfer is lower. This effect

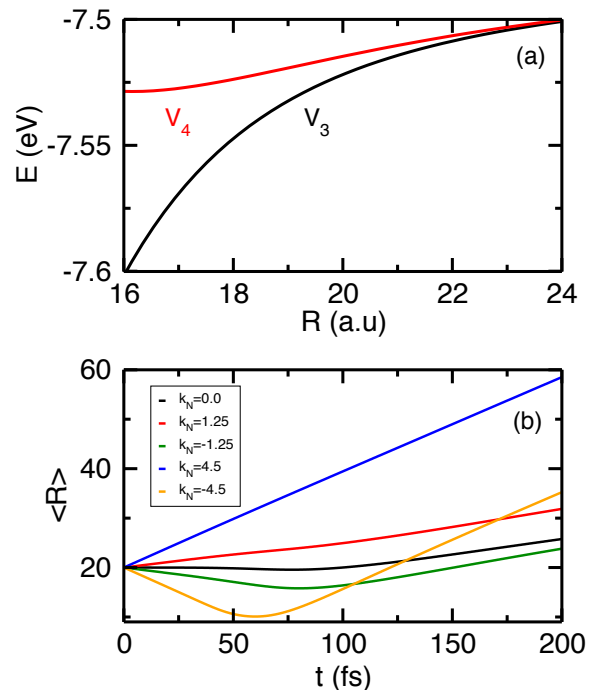


FIG. 8: (a) Potential energy curves of the second ( $V_3$ ) and third ( $V_4$ ) excited states around  $R=20$  a.u. (b) Variation of the average internuclear distance for different values of the initial average nuclear momentum. For negative values, the nuclei initially approach until a minimum value of  $\langle R \rangle$  when they collide after which the internuclear distance increases. For positive values of  $k_N$ , the nuclei always separate, at a speed that depends on  $k_N$ . (c) Overlap between the nuclear wave functions corresponding to the second,  $\psi_3$ , and third,  $\psi_4$ , excited states for different initial nuclear kinetic energies.

is more significant as the initial nuclear kinetic energy is bigger. Regarding the effect of the initial width of the nuclear wave packet, we can observe the total population remains constant but the population transfer increases as we move to lower values of initial kinetic energy. Therefore, highly localized nuclear wave packets (small widths) favor the electron transfer.

#### IV. CONCLUSIONS

We have studied electron transfer between two separated protons using Local Control Theory (LCT), in a 1D model system assuming fixed nuclei interacting through soft-core Coulomb potentials. By properly choosing the control functional, the initial conditions and the timing of the dynamics, we have searched for optical pulses that lead to electron transfer on the time-scale of hundreds of femtoseconds, achieving high yields for the overall process.

The analysis of the transfer showed that the pro-

cess was mediated by tunneling below the Coulomb barrier between the protons. Generalizing the results we have proposed control strategies where two time-delayed pulses are used first to prepare the initial state closer to the barrier whenever the protons are too largely separated (and hence the tunneling rate is too slow) and finally to de-excite the electronic state on the target proton, avoiding the backward transfer. In between the pulses the dynamics follows by laser-free tunneling, which essentially yields perfect electron transfer.

This mechanism is in contrast to recent proposals that used impulsive ultrashort pulses to mediate the transfer through the ionizing continuum[13]. In the latter case the yields were much smaller, but remained less affected by the motion of the nuclei.

Using a 2D study of the three particles moving collinearly showed that the electron transfer mediated by tunneling was severely affected by the vibrational motion of the nuclei. Since the tunneling times depend exponentially on the energy differences, the yield of electron transfer was half that observed in the 1D case even for initially frozen nuclei, simply due to the spreading of the

nuclear wave function. The effect of the remaining dimensions of the systems still needs to be evaluated, although they will likely affect in similar ways to the yield of the process. In addition, electron transfer through tunneling is more difficult to achieve in non-symmetric systems, where the ions are different. However, laser-enhanced tunneling is also a possible solution. Future studies are needed to better assert the merits of the different electron transfer mechanisms, but presumably the better choice will depend on the system of study and the initial kinetic energy of the ions.

### Acknowledgments

Financial support from the MICINN (Projects CTQ2012-36184 and CTQ2015-65033-P) and the COST-action (Grant No. CM1204, XLIC), as well as the computational facilities by CALMIP, Toulouse, are gratefully acknowledged.

- 
- [1] M. Shapiro and P. Brumer, *Quantum Control of Molecular Processes* (John Wiley & Sons, 2012).
  - [2] S. Rice and M. Zhao, *Optical Control of Molecular Dynamics* (John Wiley & Sons, 2001).
  - [3] C. Brif, R. Chakrabarti, and H. Rabitz, *Adv. Chem. Phys.* **148**, 1 (2011).
  - [4] J. A. Yeazell, M. Mallalieu, and C. R. Stroud, *Phys. Rev. Lett.* **64**, 2007 (1990).
  - [5] J. Bromage and C. R. Stroud, *Phys. Rev. Lett.* **83**, 4963 (1999).
  - [6] M. Corrales, J. González-Vázquez, G. Balerdi, I. Sola, R. de Nalda, and L. Bañares, *Nat. Chem.* **6**, 785 (2014).
  - [7] B. J. Sussman, D. Townsend, M. Y. Ivanov, and A. Stolow, *Science* **314**, 278 (2006).
  - [8] H. Timmers, Z. Li, N. Shivaram, R. Santra, O. Vendrell, and A. Sandhu, *Phys. Rev. Lett.* **113**, 113003 (2014).
  - [9] N. Došlić, O. Kühn, J. Manz, and K. Sundermann, *J. Phys. Chem. A* **102**, 9645 (1998).
  - [10] P. R. Schreiner, H. P. Reisenauer, D. Ley, D. Gerbig, C.-H. Wu, and W. D. Allen, *Science* **332**, 1300 (2011).
  - [11] B. Y. Chang, S. Shin, A. Palacios, F. Martín, and I. R. Sola, *J. Phys. B* **48**, 043001 (2015).
  - [12] B. Y. Chang, S. Shin, A. Palacios, F. Martín, and I. R. Sola, *J. Chem. Phys.* **139**, 084306 (2013).
  - [13] P. Vindel-Zandbergen, C. Meier, and I. R. Sola, *Chem. Phys.* **478**, 97 (2016).
  - [14] Z. Li, O. Vendrell, and R. Santra, *Phys. Rev. Lett.* **115**, 143002 (2015).
  - [15] F. Calegari, D. Ayuso, A. Trabatttoni, L. Belshaw, S. De Camillis, S. Anumula, F. Frassetto, L. Poletto, A. Palacios, P. Decleva, *et al.*, *Science* **346**, 336 (2014).
  - [16] D. J. Tannor, R. Kosloff, and A. Bartana, *Faraday Discuss.* **113**, 365 (1999).
  - [17] V. Engel, C. Meier, and D. J. Tannor, *Adv. Chem. Phys.* **141**, 29 (2009).
  - [18] V. S. Malinovsky and D. J. Tannor, *Phys. Rev. A* **56**, 4929 (1997).
  - [19] J. Javanainen, J. H. Eberly, and Q. Su, *Phys. Rev. A* **38**, 3430 (1988).
  - [20] Q. Su and J. H. Eberly, *Phys. Rev. A* **44**, 5997 (1991).
  - [21] K. C. Kulander, F. H. Mies, and K. J. Schafer, *Phys. Rev. A* **53**, 2562 (1996).
  - [22] T. Bredtmann, S. Chelkowski, and A. D. Bandrauk, *Phys. Rev. A* **84**, 021401 (2011).
  - [23] C. Lefebvre, H. Z. Lu, S. Chelkowski, and A. D. Bandrauk, *Phys. Rev. A* **89**, 023403 (2014).
  - [24] S. Gräfe, M. Erdmann, and V. Engel, *Phys. Rev. A* **72**, 013404 (2005).
  - [25] R. Kitzer, C. Meier, and V. Engel, *Chem. Phys. Lett.* **477**, 75 (2009).
  - [26] M. Feit, J. Fleck Jr., and A. Steiger, *J. Comp. Phys.* **47**, 412 (1982).
  - [27] M. D. Feit, *J. Chem. Phys.* **78**, 301 (1983).
  - [28] M. D. Feit and J. A. Fleck, *J. Chem. Phys.* **80**, 2578 (1984).
  - [29] D. Macias, S. Brouard, and J. Muga, *Chem. Phys. Lett.* **228**, 672 (1994).
  - [30] J. Palao and J. Muga, *Chem. Phys. Lett.* **292**, 1 (1998).
  - [31] C. C. Marston and G. G. Balint-Kurti, *J. Chem. Phys.* **91**, 3571 (1989).
  - [32] K. Husimi, *Proc. Phys. Math. Soc. Jpn* **22**, 264 (1940).